Supported Bilayers with Excess Membrane Reservoir: A Template for Reconstituting Membrane Budding and Fission

Thomas J. Pucadyil* and Sandra L. Schmid*
Department of Cell Biology, Scripps Research Institute, La Jolla, California

ABSTRACT A complete mechanistic understanding of membrane-localized processes in vesicular transport, such as membrane budding and fission, requires their reconstitution with biochemically-defined components from a biochemically-defined substrate. Supported bilayers formed by vesicle fusion represent an attractive substrate for this purpose. However, conventional supported bilayers lack a sufficient membrane reservoir to recreate membrane budding and fission events. We describe the formation of supported bilayers with excess membrane reservoir (SUPER) templates from the fusion of liposomes containing negatively charged lipids on silica beads under high-ionic-strength conditions. Using a fluorescence microscopy-based assay to monitor early and late stages of supported bilayer formation, we show that an increase in ionic strength leads to an increase in the rates of liposome adsorption and subsequent fusion during formation of supported bilayers. The two rates, however, increase disproportionally, leading to accumulation of excess reservoir with an increase in ionic strength. SUPER templates allow the seamless application of microscopy-based assays to analyze membrane-localized processes together with sedimentation-based assays to isolate vesicular and nonvesicular products released from the membrane. The results presented here emphasize the general utility of these templates for analyzing vesicular and nonvesicular transport processes.

INTRODUCTION

Vesicular transport is a process by which cells take up nutrients from the extracellular environment, generate organelles, and maintain the compositional identity of cellular membranes. This process exhibits diversity in terms of the vesicular intermediates it generates and the type of cargo that is sorted and captured in transport intermediates. During coated-vesicular transport, protein coats assembled from cytosolic constituents form around and encapsulate the underlying membrane to generate vesicles that are used to efficiently sort and traffic transmembrane cargo (1–3). Transport pathways that generate tubulovesicular intermediates lacking a discernible coat traffic fluid and bulk membrane from one cellular compartment to another (4).

Reconstituting vesicular transport in a biochemically-defined system is a powerful approach for deciphering first principles and gaining mechanistic insight into this cellular process. Liposomes were the preferred membrane reservoir in earlier vesicular transport reconstitution studies (5,6), and our current understanding of this cellular process is largely based on the insights provided by those studies. However, liposomes present inherent limitations to the analysis of reactions involving membrane budding and fission. Their small size precludes spatially resolved, dynamic analyses using techniques such as fluorescence microscopy, and their buoyancy necessitates a density-gradient analysis to isolate the end products of a vesiculation process. The latter is of particular concern because osmotic imbalances that would be experienced during density-gradient runs could sever meta-stable transport intermediates, as was recently described for membrane tethers (7). Moreover, membrane templates with the capacity of displaying gradients of membrane curvature in the form of buds on an otherwise planar surface would be desirable because membrane curvature appears to be an important determinant in spatially regulating the activities of proteins in vesicular transport (8). Recreating the gradients of membrane curvature requires liposome preparations larger than the typical dimensions of transport vesicles (~100 nm). However, the heterogeneity in size of the liposomes associated with such preparations makes them poorly suited for this purpose.

Supported bilayers have emerged as a popular model membrane system and have been used to reconstitute multiple membrane-localized processes, such as cell signaling, cell-cell communication, and soluble *N*-ethylmaleimide sensitive factor attachment protein receptor- and virus-mediated membrane fusion events (9,10). Supported bilayers are formed by the spontaneous reorganization of surface-adsorbed liposomes into planar bilayers on solid supports (11–13). A combination of hydration, van der Waals, and electrostatic forces retains the bilayer on the surface. Of importance, constituent lipid molecules in supported bilayers diffuse laterally because the bilayer is separated from the solid support by a thin (1–2 nm) aqueous cushion (14).

We previously described the supported bilayers with excess membrane reservoir (SUPER) template and discussed its use in analyzing membrane fission and vesicle release catalyzed by the large GTPase dynamin-1 (15). Here, we present a detailed characterization of these templates in terms of accumulation of excess membrane reservoir, and assess

Submitted February 17, 2010, and accepted for publication April 19, 2010.

*Correspondence: pucadyil@gmail.com or SLSchmid@scripps.edu

Thomas J. Pucadyil's present address is Indian Institute of Science Education and Research, Pune, Maharashtra, India.

Editor: Petra Schwille.

0006-3495/10/07/0517/9 $2.00

doi: 10.1016/j.bpj.2010.04.036

their robustness as templates for analyzing biologically relevant vesiculation events.

MATERIALS AND METHODS

Preparation of liposomes

Stock solutions of 1,2-dioleoyl-*sn*-glycero-3-phosphocholine (DOPC), 1,2-dioleoyl-*sn*-glycero-3-phospho-L-serine (DOPS), 1,2-dioleoyl-*sn*-glycero-3-phosphoethanolamine (DOPE), cholesterol, L-α-phosphatidylinositol-4,5-bisphosphate (ammonium salt, PI-(4,5)-P_2), 1,2-dioleoyl-*sn*-glycero-3-phosphoethanolamine-N-(lissamine rhodamine B sulfonyl) (ammonium salt, RhPE), and 1,2-dioleoyl-*sn*-glycero-3-phosphoethanolamine-N-(7-nitro-2-1,3-benzoxadiazol-4-yl) (ammonium salt, NBD-PE) were obtained from Avanti Polar Lipids (Alabaster, AL). The required volumes from stock solutions were aliquoted into a glass tube and mixed gently. The solvent was dried rapidly under a stream of nitrogen while it was gently warmed (~50°C). The lipids were further dried under hard vacuum for 30 min. The dried lipids were hydrated in water filtered through a Milli-Q system (Millipore, Bedford, MA) for 30 min at 50°C with intermittent vortexing. To prepare small unilamellar vesicles (SUVs), hydrated lipids were sonicated with a probe sonicator (Thermo Fisher Scientific, Waltham, MA) at a low-amplitude setting in an ice-water mixture. The samples were centrifuged at 100,000 *g* for 20 min at room temperature and the supernatant was collected. Large unilamellar vesicles (LUVs) were prepared by subjecting the hydrated lipids to multiple freeze-thaw cycles using liquid N_2 before extruding them through 0.1 μm polycarbonate filters using an Avanti Mini-extruder. The final phospholipid concentration was determined by assaying the phosphate content subsequent to total digestion by perchloric acid (16).

Preparation of templates

Silica beads (4.9 μm diameter; Corpuscular Inc., Cold Spring, NY) were added to a premixed solution of liposomes with the desired NaCl concentration in a total volume of 100 μL in a 1.5 mL clear polypropylene centrifuge tube. The final bead density and liposome concentration were 5×10^6 and 200 μM, respectively. This mixture was incubated for 30 min at room temperature with intermittent vortexing. The templates thus formed were washed four times with 1 mL of water by a low-speed spin (300 *g*) for 2 min in a swinging bucket rotor at room temperature, leaving behind a 100 μL volume of water in each wash. We avoided the use of buffers during template formation because our goal was to analyze the specific effect of salt on supported bilayer formation, and the buffers themselves contribute substantially to the ionic strength. However, the results were qualitatively similar to those obtained from templates formed with salt solutions buffered with 20 mM HEPES pH 7.5.

Dynamin expression and purification

Dynamin-1 was expressed and purified as described previously (17).

Sedimentation assays with templates

Membrane (lipid) released from RhPE-labeled templates was analyzed by means of a sedimentation assay. Briefly, an aliquot (10 μL) of templates was gently added without mixing to 20 mM HEPES pH 7.5, 150 mM NaCl buffer (90 μL) in 1.5 mL polypropylene centrifuge tubes. In a separate reaction, we estimated the total lipid concentration on the templates by adding them to buffer containing 0.1% Triton X-100. The samples were left undisturbed for 30 min at room temperature, and the beads were spun down at low speed (300 *g*) for 2 min at room temperature. An aliquot (75 μL) of the supernatant was mixed with 25 μL of 0.4% Triton X-100 (Thermo Fisher Scientific, Waltham, MA) or, to estimate the total lipid, 0.1% Triton X-100. The fluorescence intensity of the supernatant was read in a plate reader (Bio-Tek Instruments, Winooski, VT) using 530/25 nm excitation and 590/25 nm emission filters. Membrane fission assays were carried out with 0.5 μM dynamin-1 in 20 mM HEPES pH 7.5, 150 mM NaCl, 1 mM $MgCl_2$ buffer with 1 mM GTP (Axxora, San Diego, CA). Template stability assays were carried out with increasing concentrations of Triton X-100 or with fatty acid-free bovine serum albumin (BSA; Roche, Indianapolis, IN) in 20 mM HEPES pH 7.5, 150 mM NaCl buffer.

Fluorescence microscopy

Glass coverslips (Fisher Scientific, Pittsburgh, PA) were cleaned with piranha solution (conc. H_2SO_4/30% H_2O_2 4:1, v/v) for 1 h at room temperature and washed extensively with boiling water. The coverslips were allowed to attain room temperature, stored under water, and air-dried before use. To coat the coverslips with PEG-silane, piranha-cleaned coverslips were first dried in an oven at 200°C for 3 h and then treated at room temperature for 30 min with PEG-silane (2%, v/v; Gelest Inc., Morrisville, PA) in acetone. The coverslips were later washed extensively with water and air-dried before use. Templates and liposomes were imaged on an inverted Olympus IX-71 microscope equipped with a Hamamatsu ORCA ER 1392 CCD camera with a 100×, 1.4 NA, oil-immersion objective using 555/28 nm excitation and 600/30 nm emission filters. Fluorescence images were analyzed using ImageJ (http://rsb.info.nih.gov/ij/). Dithionite quenching experiments were performed as described previously (15).

RESULTS

Effect of ionic strength on the membrane reservoir in negatively charged supported bilayers

A prerequisite for vesicular transport is a fluid membrane reservoir that is capable of undergoing budding and fission to generate vesicles. Conventional supported bilayers are not ideal substrates for vesicle formation because interactions between the lipid bilayer and the solid support tend to reduce the propensity for the bilayer to undergo shape transformations. Previous studies showed that supported bilayers formed with phosphatidic acid (PA)-containing liposomes under high-ionic-strength conditions display budded membrane structures (18–20). This effect was attributed to phase separation under conditions of high ionic strength due to the intrinsic negative charge and curvature of PA. However, we reasoned that the budded membrane structures could also have formed as the result of an increased membrane reservoir in the supported bilayers, which may have been due to the inclusion of negatively charged lipids in the mixture. To test this, we systematically examined the influence of ionic strength and negatively charged lipid content on the membrane reservoir in supported bilayers. We chose to use silica beads as the substrate on which to form supported bilayers because the membrane reservoir can be readily quantified by a low-speed spin that sediments beads and removes unbound liposomes. Supported bilayers were formed by fusion of DOPC/DOPS (85:15 mol%) SUVs (200 μM) in the presence of increasing concentrations of NaCl. The liposomes contained a trace amount (1 mol%) of a fluorescent lipid analog, RhPE, for detection purposes. The templates thus formed were washed several times by low-speed sedimentation and resuspension in water to

remove unbound SUVs and excess salt. The membrane reservoir in the templates was estimated based on the RhPE fluorescence released with 0.1% Triton X-100. Fig. 1 *A* shows that an increase in ionic strength of the medium during template formation leads to a significant increase in the membrane reservoir deposited on the templates. Thus, the templates accumulate a 2.5-fold excess reservoir with an increase in NaCl concentration from 1 mM to 1 M.

To visualize the membrane reservoir, we added beads to a drop of phosphate-buffered saline solution on a piranha-cleaned glass coverslip. The templates bind and spontaneously spill out their excess reservoir, which can be seen as a patch of membrane around the templates when imaged at their basal plane (Fig. 1 *B*, *arrows*). The fluorescence intensity of templates should be proportional to the membrane reservoir on them; therefore, we analyzed the amount of membrane reservoir on individual templates by fluorescence microscopy. Fig. 1 *C* shows templates focused at the equatorial plane of the beads formed with 1 mM NaCl and those formed with 1 M NaCl, before and after their excess reservoir spilled onto the glass coverslip. The templates formed with 1 M NaCl have a 2.4-fold higher fluorescence intensity than those formed with 1 mM NaCl (Fig. 1 *D*), consistent with bulk fluorescence measurements (Fig. 1 *A*). Of importance, spillage of the excess reservoir from templates formed with 1 M NaCl reduces their intensity to levels seen in templates formed with 1 mM. These results indicate that the excess membrane reservoir can be depleted by external manipulations, such as allowing it to spread out on a glass surface, and suggest that the reservoir is organized as a single bilayer with folds rather than multiple lamellae stacked together. We analyzed this by monitoring the accessibility of the fluorescent lipid analog NBD-PE to quenching by dithionite, a water-soluble reducing agent. Fig. 1 *E* shows that ~70% of the NBD-PE fluorescence in the reservoir is quenched by dithionite, suggesting a unilamellar membrane. In comparison, LUVs of the same lipid composition showed ~60% quenching of fluorescence by dithionite (Fig. 1 *E*). The higher degree of quenching with templates could be due to the presence of submicroscopic defects that are more permeable to dithionite than the bulk of the supported bilayer.

Effect of negatively charged lipids on the membrane reservoir in supported bilayers

The above results show that an increase in the NaCl concentration leads to an increase in the membrane reservoir in templates formed with a fixed DOPS content. We next tested the effect of varying the DOPS content on the membrane reservoir in templates at fixed NaCl concentrations. Fig. 2 *A* shows that at 1 mM NaCl, increasing the DOPS content tends to reduce the reservoir on templates, and this effect reaches saturation at 9 mol% DOPS (Fig. 2 *A*, *open circles*). The opposite is seen when templates are formed in the presence of 1 M NaCl, i.e., an increase in the DOPS content leads to an increase in the membrane reservoir (Fig. 2 *A*, *solid circles*). Thus, under high-ionic-strength conditions, the inclusion of DOPS results in an increase in membrane reservoir on the templates (Fig. 2 *B*), reaching a maximum of

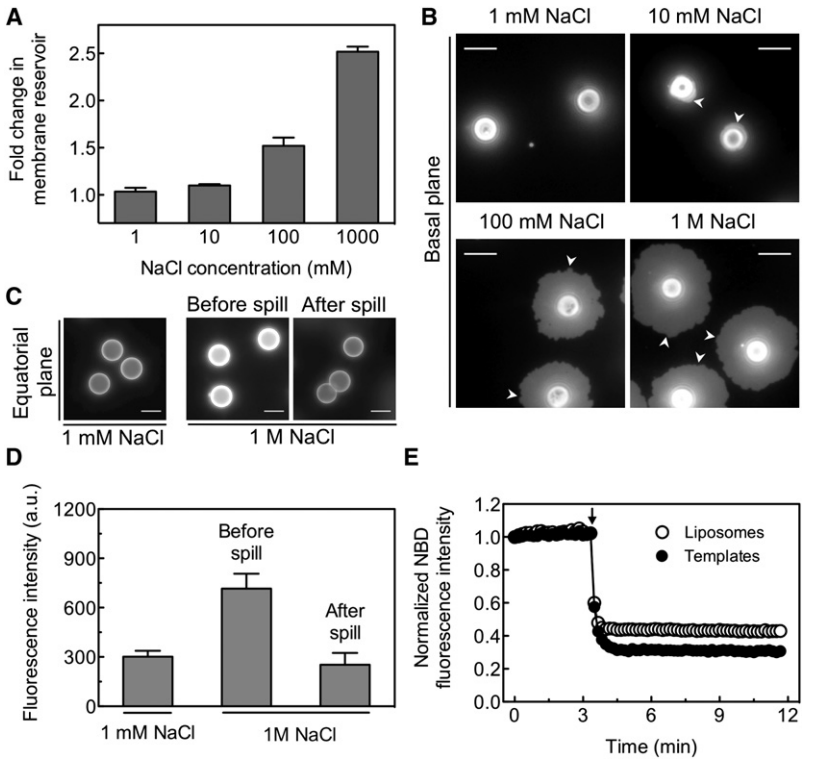

FIGURE 1 (*A*) Fold change in the membrane reservoir in templates formed with DOPC/DOPS/RhPE (84:15:1 mol%) with increasing concentrations of NaCl. Data represent the mean ± SD ($n = 4$). Templates were formed on silica beads with 200 μM SUVs and washed extensively to remove unbound SUVs and excess salt, and subsequently solubilized in 0.1% Triton X-100 to estimate the amount of membrane reservoir. (*B*) Fluorescence images of templates formed with the indicated concentrations of NaCl and added to a piranha-cleaned glass coverslip. Templates were imaged at their basal plane to visualize the spread of membrane reservoir on to the coverslip (*arrows*). Scale bars = 5 μm. (*C*) Fluorescence images of templates formed with 1 mM NaCl and 1 M NaCl, before and after the membrane reservoir spread out. Templates were imaged at their equatorial plane. Scale bars = 5 μm. (*D*) Fluorescence intensities of templates analyzed from images acquired under conditions shown in *C*. Data represent the mean ± SD ($n \geq 36$ templates for each condition). (*E*) Dithionite-induced quenching of fluorescence in LUVs and templates formed with 1 M NaCl composed of DOPC/DOPS/NBD-PE (83:15:2 mol%). The arrow marks the time of dithionite addition. Values are normalized to the fluorescence intensity before dithionite addition and represent the mean of five experiments.

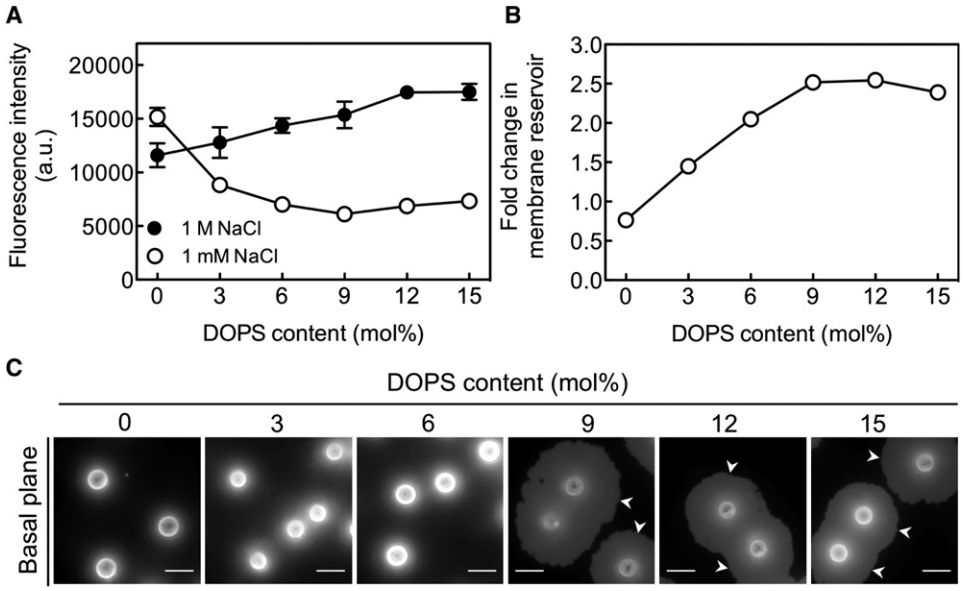

FIGURE 2 (*A*) Membrane reservoir in templates formed with SUVs of increasing DOPS content in the presence of 1 mM and 1 M NaCl. Data represent the mean ± SD ($n = 3$). (*B*) Fold change in the membrane reservoir in templates with increasing DOPS content. Data represent the ratio of fluorescence intensities in templates formed with 1 M and 1 mM NaCl shown in panel *A*. (*C*) Fluorescence images of templates formed with 1 M NaCl with SUVs of increasing DOPS content deposited on a glass coverslip. Templates were imaged at their basal plane to visualize the spread of the membrane reservoir onto the coverslip (*arrows*). Scale bars = 5 μm.

~2.4-fold at 9 mol% DOPS. Fig. 2 *C* shows images of the reservoir spilled onto glass coverslips from templates formed with increasing concentrations of DOPS in the presence of 1 M NaCl. Of interest, the reservoir around the templates spreads out only when the DOPS content is 9 mol% or higher. We note that the reservoir in templates containing 15 mol% DOPS and formed in 1 M NaCl (Fig. 2 *A*, ~16,000 a.u.) is similar to that seen in DOPC templates formed with 1 mM NaCl (Fig. 2 *A*, ~15,000 a.u.), yet we did not observe any membrane spreading on coverslips from the latter (data not shown). This indicates that the high salt increases the reservoir in negatively charged templates to levels seen in zwitterionic templates, and that the spreading of the reservoir from templates on to the glass surface depends on both the membrane reservoir and the presence of negatively charged lipids.

Kinetic analysis of supported bilayer formation

We monitored the kinetics of template formation to gain insight into the mechanism by which salt increases the membrane reservoir in negatively charged templates. Silica beads were incubated with DOPC/DOPS (85:15 mol%) SUVs in the presence of increasing NaCl concentrations for different periods of time. The templates attained their characteristic reservoir within 5 min, the shortest time point possible with the sedimentation assay, and remained constant for up to 60 min (data not shown). From this, we conclude that the buildup of excess reservoir on the templates was due to events occurring during supported bilayer formation, rather than to vesicles fusing to an already formed supported bilayer.

To further define the mechanism behind the salt-dependent deposition of excess reservoir, we developed quantitative assays to measure the early events in supported bilayer formation. For these assays, low concentrations of fluorescently labeled LUVs (DOPC/DOPS/RhPE (84:15:1 mol%, 2 μM) were added to glass coverslips and visualized by epifluorescence microscopy. The adsorption of LUVs can be seen by the appearance of fluorescent punctae on the glass surface (Fig. 3 *A*, *arrows* in *top* and *bottom panels* at t = 1.3 s) that increase in number with time in the absence of excess unlabeled SUVs (Fig. 3 *A*, *top panel*). The low concentration of fluorescent LUVs used in these experiments allowed us to monitor events taking place on the coverslip surface without significant interference from fluorescence in the bulk solution. Performing the same experiment in the presence of a 100-fold excess of unlabeled SUVs (DOPC/DOPS 85:15 mol%, 200 μM) allowed us to visualize supported bilayer formation. Under these conditions, the adsorbed, fluorescently labeled LUVs transform into irregular, lower-intensity patches, suggesting spreading due to fusion with unlabeled SUVs and subsequent dilution of the fluorescent lipid (see Fig. 3 *A*, *bottom panel* at t = 23.4 s, and Movie S1 in the Supporting Material for the entire sequence). Note that the spread is limited at this stage, and hence the patch boundaries can still be clearly distinguished. The patches are heterogeneous in size and fluorescence intensity. With time, the fluorescence in the patches continues to decrease as they appear to expand and merge with adjacent ones. Eventually the entire field becomes homogeneous, reflecting the formation of a continuous supported bilayer. A similar trend was seen with DOPC liposomes (data not shown), implying that the formation of such kinetic intermediates is a characteristic feature of supported bilayer formation. Quantitation of these data showed that the fluorescence intensity of LUVs remained constant in the absence but dropped in the presence of excess unlabeled SUVs (Fig. 3 *B*), indicating that the imaging parameters were optimized to avoid photobleaching of the fluorescent lipid, and that the loss of intensity was indeed due to fusion.

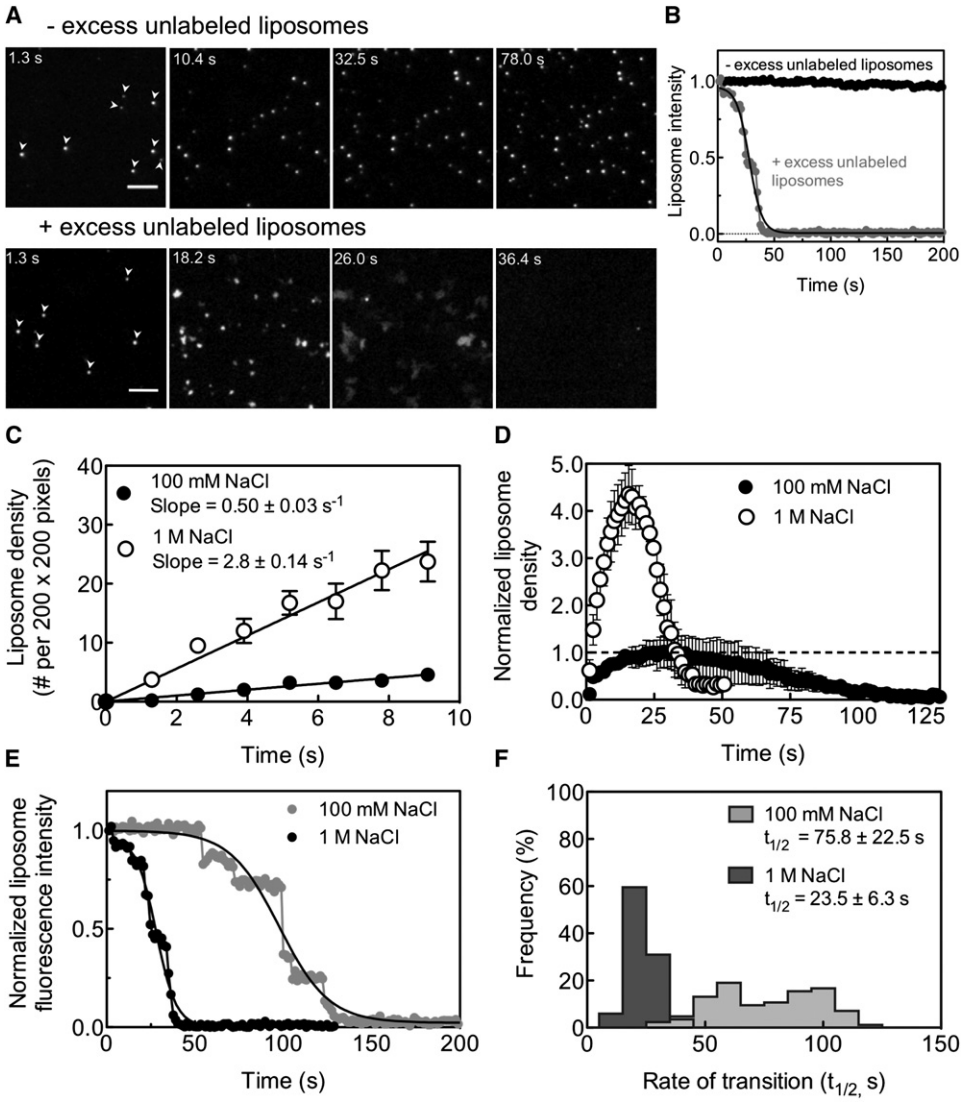

FIGURE 3 (*A*) Microscopy-based assay to monitor the kinetics of liposome adsorption and formation of supported bilayers on glass coverslips. The assay is initiated by adding a 20 μL aliquot of 2 μM fluorescent LUVs composed of DOPC/DOPS/RhPE (84:15:1 mol%) in the absence (for adsorption, *top panel*) or presence (for supported bilayer formation, *bottom panel*) of 200 μM of unlabeled SUVs composed of DOPC/DOPS (85:15 mol%) to a 1 cm wide circle (marked by a permanent marker) on a piranha-cleaned glass coverslip. Top panel: Time-lapse sequence showing the adsorption of fluorescent LUVs (*arrows* in panel t = 1.3 s) to the glass coverslip. Bottom panel: The same in the presence of unlabeled SUVs, showing both adsorption and fusion to form a supported bilayer. Scale bar = 5 μm. See Movie S1 for the entire sequence. (*B*) Fluorescence intensity of a single fluorescent LUV in the absence (*black circles*) and presence (*gray circles*) of excess unlabeled SUVs. (*C*) Kinetics of adsorption of fluorescent LUVs in the presence of 100 mM (*black circles*) and 1 M (*white circles*) NaCl. Data represent the mean ± SD ($n = 6$). (*D*) Kinetics of adsorption of fluorescent LUVs (rising phase), their fusion with unlabeled SUVs (declining phase), and the formation of a supported bilayer in the presence of 100 mM (*black circles*) and 1 M (*white circles*) NaCl. Values are normalized to the peak in liposome density reached with 100 mM NaCl (*dotted line*). Data represent the mean ± SE ($n = 3$). (*E*) Representative traces showing the loss in fluorescence intensities associated with the transition of single LUVs to supported bilayers in the presence of 100 mM (*gray circles*) and 1 M (*black circles*) NaCl. The decay in fluorescence intensity occurs in discreet stages, as shown by the step-like drop in intensity. The complete decay process was fit to a sigmoidal curve to determine the rate ($t_{1/2}$) of transition to a supported bilayer. (*F*) Histograms of the $t_{1/2}$ of the liposome-to-supported-bilayer transition in the presence of 100 mM and 1 M NaCl. Data represent the mean ± SD ($n = 84$).

We analyzed time-lapse sequences acquired in the absence of excess unlabeled SUVs for rates of liposome adsorption by tracking the number of fluorescent LUVs present at each frame. We monitored the adsorption of DOPC/DOPS (85:15 mol%) liposomes in the presence of 100 mM and 1 M NaCl, conditions that lead to a 1.7-fold increase in membrane reservoir (Fig. 1 *A*). Of importance, the rate of adsorption of liposomes is highly sensitive to the ionic strength. Thus, an increase in NaCl concentration from 100 mM to 1 M results in a ~6-fold increase in the rate of liposome adsorption (Fig. 3 *C*, slope = 0.50 ± 0.03 s^{-1} for 100 mM NaCl and 2.80 ± 0.14 s^{-1} for 1 M NaCl). We analyzed time-lapse sequences in the presence of excess unlabeled SUVs for rates of supported bilayer formation by tracking the decay in fluorescence intensity of individual LUVs. At the ensemble level, liposome adsorption can be seen as a rising phase, whereas the subsequent fusion of the liposomes creates a declining phase until a low-intensity plateau is reached, indicative of supported bilayer formation (Fig. 3 *D*). Again, the rate and extent of adsorption of liposomes in the presence of 1 M NaCl is significantly increased as compared to that seen with 100 mM NaCl. As expected, this higher liposome density results in the subsequent liposome fusion events (i.e., the declining phase) being both faster and more cooperative than those seen with 100 mM NaCl. Thus, the formation of supported bilayers is completed in a shorter period of time with 1 M NaCl (~40 s) than with 100 mM NaCl (~100 s). These effects were more accurately quantified by analyzing the liposome-to-supported-bilayer transformation at the level of single liposomes (Fig. 3, *E*

and *F*). The decay in fluorescence intensity of a single adsorbed liposome during supported bilayer formation occurs in discrete stages, as evidenced by the step-like drop in intensity (Fig. 3 *E*). These data were fit to a sigmoidal function to estimate the rate ($t_{1/2}$) of liposome-to-supported-bilayer transformation (Fig. 3 *E*, *smooth traces*). Consistent with the ensemble measurements, the kinetics of supported bilayer formation was ~3-fold faster in 1 M NaCl than in 100 mM NaCl (Fig. 3 *F*, $t_{1/2} = 23.5 \pm 6.3$ s for 1 M NaCl and 75.8 ± 22.5 s for 100 mM NaCl, $n = 84$). In addition, fusion events occurred with greater cooperativity, as reflected by the narrower distribution of half-lives seen with 1 M compared to 100 mM NaCl (Fig. 3 *F*). The kinetics of formation of supported bilayers with DOPC was insensitive to the salt concentration (data not shown). Together, these data demonstrate that the salt-dependent accumulation of excess reservoir in negatively charged templates occurs primarily as a consequence of the initial increase in the rate of adsorption of liposomes to the glass/silica surface.

Membrane remodeling of SUPER templates

The large GTPase dynamin-1 is involved in a number of transport processes that occur at the plasma membrane, where it recognizes specific lipids such as PI-(4,5)-P_2 (21). To study its effects on SUPER templates, we first analyzed templates formed with a lipid composition that mimicked the inner leaflet of the plasma membrane in terms of lipid headgroup characteristics. Fig. 4 *A* shows the fold increase in membrane reservoir in templates composed of DOPC/DOPE/cholesterol/DOPS/PI-(4,5)-P_2/RhPE (26:20:33:15:5:1 mol%) with increasing NaCl concentrations. Thus, the templates accumulate 2.5-fold more reservoir when formed in the presence of 1 M NaCl compared to 30 mM NaCl, the lowest NaCl concentration necessary to form templates with cholesterol-containing liposomes. Again, the excess membrane reservoir spreads out from these templates onto a glass coverslip (Fig. 4 *B*, *arrows*). These results are similar to those observed for templates composed of relatively simple lipid mixtures of DOPC/DOPS (85:15 mol%; Fig. 1, *A* and *B*), and hence demonstrate the feasibility of generating SUPER templates with diverse lipid compositions.

The ability to microscopically visualize templates while they are in suspension and to isolate the end products of a vesiculation reaction by a low-speed spin forms the basis of a facile assay to analyze the function of proteins involved in membrane remodeling events. This was demonstrated recently in a study that analyzed the effects of dynamin-1

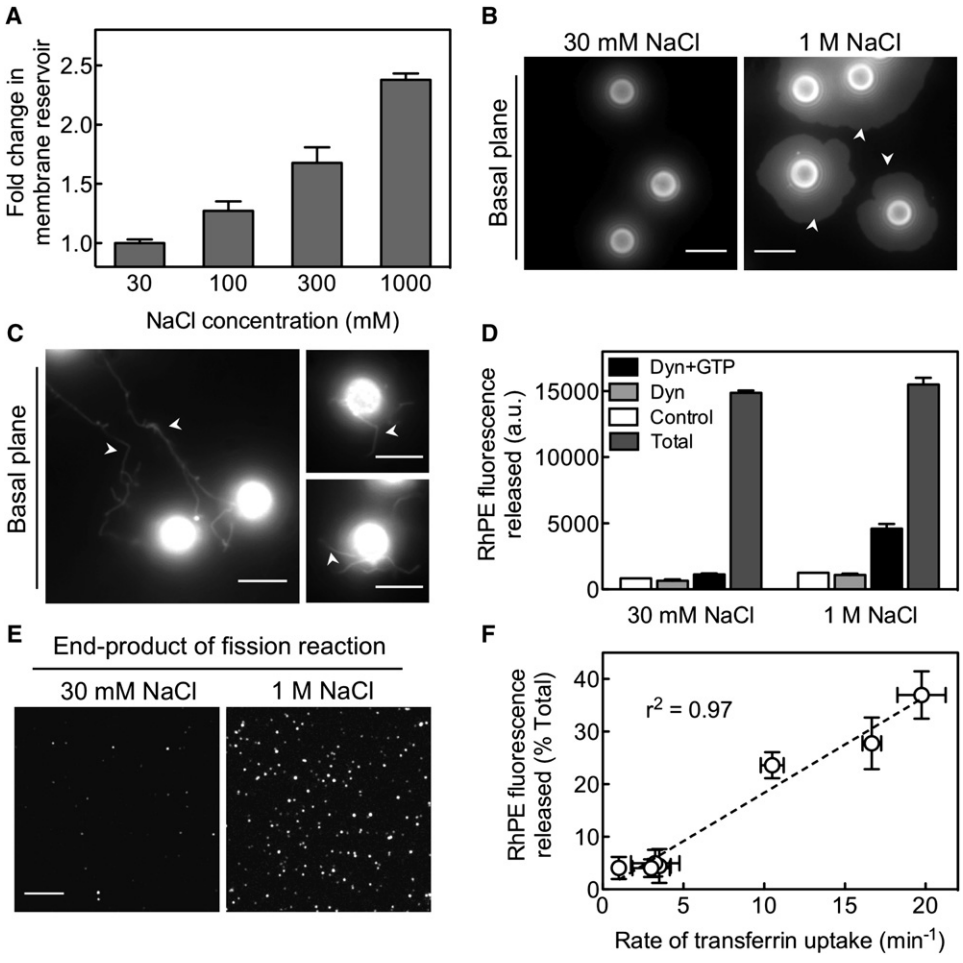

FIGURE 4 (*A*) Fold change in the membrane reservoir with increasing concentrations of NaCl in templates formed with DOPC/DOPE/cholesterol/DOPS/PI-(4,5)-P_2/RhPE (26:20:33:15:5:1 mol%) SUVs. Data represent the mean ± SD ($n = 3$). (*B*) Fluorescence images of templates formed with the indicated concentrations of NaCl deposited on a glass coverslip. The microscope focus was adjusted to the basal plane of the templates to visualize the spread of the membrane reservoir onto the coverslip (*arrows*). Scale bars = 5 μm. (*C*) Dynamin-induced membrane tubule formation (*arrows*) from templates formed with 1 M NaCl. Experiments were carried out on PEG-silane-coated coverslips to prevent the excess reservoir from spreading out of the templates. (*D*) Efficiency of GTP-dependent, dynamin-catalyzed membrane fission and vesicles release with templates formed with the indicated NaCl concentrations. Data represent the mean ± SD ($n = 3$). (*E*) Fluorescence micrograph of vesicles in the supernatant from a dynamin-catalyzed membrane fission assay carried out on templates formed with the indicated concentrations of NaCl. (*F*) Correlation between membrane fission (RhPE fluorescence released into supernatant) and rate of clathrin-mediated endocytosis monitored by transferrin uptake in cells for wild-type and six different dynamin-1 point mutants.

on templates composed of DOPC/DOPS/PI-(4,5)-P_2 (80:15:5 mol%) (15). In the absence of GTP, dynamin-1 self-assembles to remodel the membrane into long tubules, whereas in the presence of GTP, self-limited assemblies of dynamin catalyze fission and concomitant release of vesicles from templates. To determine the significance of the excess reservoir for such membrane remodeling events, we analyzed dynamin-mediated tubule formation and vesicle release from templates formed in the presence of either 30 mM or1 M NaCl. Fig. 4 *C* shows that in the absence of GTP, the addition of 0.5 μM dynamin-1 to SUPER templates leads to the formation of long membrane tubules (Fig. 4 *C*, *arrows*). Similar experiments with templates formed in the presence of 30 mM NaCl did not produce any membrane tubules (data not shown), indicating that excess membrane reservoir is indeed necessary for dynamin-self assembly and tubule formation. Fig. 4 *D* shows that in the presence of 1 mM GTP, 0.5 μM dynamin-1 catalyzes the release of 30% of the total RhPE fluorescence in templates formed with 1 M NaCl. Even though the total lipid was kept constant in the assay, the RhPE release from templates formed with 30 mM NaCl (7%) is only barely detectable over the background fluorescence (5%) in samples with templates alone (control), or with dynamin in the absence of GTP. This background likely originates from residual SUVs left over from template preparation. Thus, a 2.5-fold increase in the membrane reservoir in templates leads to a >10-fold increase in the extent of dynamin-catalyzed membrane fission and vesicle release. The released vesicles can be microscopically visualized by adsorbing them onto a glass coverslip. Fig. 4 *E* shows vesicles generated from templates formed with 30 mM and 1 M NaCl in the presence of 0.5 μM dynamin-1 and 1 mM GTP. Consistent with the result from the sedimentation assay (Fig. 4 *D*), the presence of excess reservoir on the templates dramatically improves the efficiency of the dynamin-catalyzed vesiculation process.

Taken together, these results signify the importance of the excess membrane reservoir in templates for the successful reconstitution of vesicular transport. In addition, the extent of membrane fission in the presence of dynamin and GTP from cholesterol-containing templates (30%) is similar to that reported earlier for SUPER templates lacking cholesterol (15,17,22). Thus, the presence of cholesterol and phosphatidylethanolamine in the membrane does not significantly influence the efficiency of dynamin-catalyzed membrane fission. In cells, dynamin catalyzes the scission of clathrin-coated pits to release coated vesicles, whereas in the in vitro membrane fission assay, dynamin catalyzes the release of lipid vesicles. To determine whether the vesiculation seen with dynamin in vitro indeed mimics its cellular function, we correlated the rate of transferrin uptake (a marker for clathrin-mediated endocytosis) and membrane fission activity for wild-type and six different, previously described dynamin-1 point mutants (17,22). Fig. 4 *F* shows that these two functions are well correlated ($r^2 = 0.97$), providing confidence in the use of templates to analyze dynamin functions in particular and vesicular transport in general.

Stability of SUPER templates

We next monitored the detergent-induced solubilization and concomitant release of lipids from templates. In principle, lipid release should coincide with the critical micellar concentration (CMC) of the detergent, and no lipid release should occur at concentrations below the CMC, despite extensive membrane destabilization caused by partitioning of detergent monomers into the lipid bilayer. Sedimentation assays with a range of detergent concentrations should therefore inform us about the general stability of these templates and the possible effects of experimental manipulations, such as the low-speed spin in promoting lipid release, especially when poised to undergo solubilization. Fig. 5 *A* shows the Triton X-100-induced solubilization measured by the amount of RhPE fluorescence present in the supernatant after a low-speed spin. The fluorescence release occurs within a narrow range of detergent concentrations, with half-maximal release seen at 0.019% (v/v), in excellent agreement with the reported CMC of 0.018% (w/v) (23). Of note, templates incubated in the presence of sub-CMC concentrations (at 0.01%, v/v) do not show any significant fluorescence release despite the gross morphological changes, such as the formation of large membrane buds, on templates seen at this concentration (Fig. 5 *A*, *inset*). The lipid release therefore coincides with solubilization and not with membrane destabilization, and serves as an important control to emphasize the general stability of these SUPER templates against membrane-perturbing agents.

We also monitored the stability of SUPER templates against protein-induced membrane perturbation by testing the effect of fatty acid-free BSA. As shown in Fig. 5 *B*, DOPC templates were highly unstable in the presence of BSA, with 60% of RhPE fluorescence released at 5 μM (0.03% w/v) BSA. Of importance, templates with 12–15 mol% DOPS were resistant to the effects of BSA. BSA is well known for its tendency to delipidate membranes and act as a lipid transfer protein. However, these effects were not limited to BSA. Templates lacking DOPS were unstable even in the presence of casein and GTPase-defective mutants of dynamin-1 (data not shown). Thus, the presence of negatively charged lipids in the templates contributes substantially to the stability of the lipid bilayer. Although we do not understand the reason for the instability seen with DOPC templates, our results caution against the use of templates with low amounts of negatively charged lipids in vesicular transport assays.

DISCUSSION

We have provided a detailed characterization of the requirements for and mechanisms underlying the formation of supported bilayers with excess reservoir. These SUPER

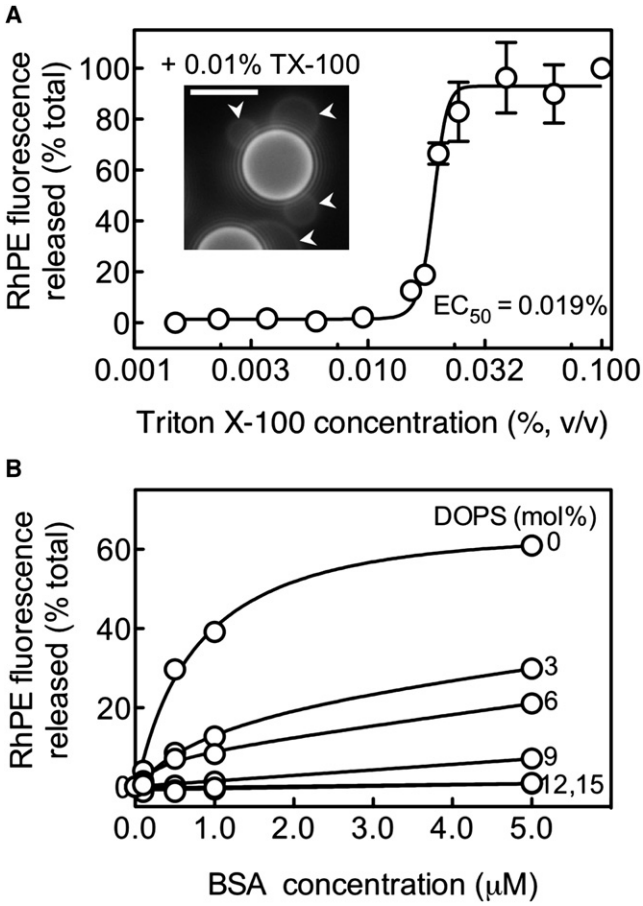

FIGURE 5 (*A*) Triton X-100-induced solubilization of the membrane bilayer on templates. Templates were formed with DOPC/DOPS/RhPE (84:15:1 mol%) SUVs in the presence of 1 M NaCl. RhPE fluorescence released into solution with increasing concentrations of Triton X-100 is plotted. Values are normalized to the fluorescence intensity in the presence of 0.1% Triton X-100 (Total). Data represent the mean ± SD ($n = 3$). Inset shows an image of templates in the presence of a sub-CMC (0.01%) concentration of Triton X-100. Templates were imaged at their equatorial plane to visualize large buds formed on them (*arrows*). Scale bar = 5 μm. (*B*) Stability of the membrane bilayer on templates against BSA. Values are normalized to the fluorescence intensity released in the presence of 0.1% Triton X-100 (% Total).

templates represent valuable new tools for studying membrane dynamics, in particular membrane budding and fission. Formation of these SUPER templates, which can incorporate multiple lipid species, requires high salt and negatively charged lipids.

The effect of ionic strength on the formation of supported bilayers composed of zwitterionic lipids has been well studied. The presence of salt has been interpreted to alter the pathway by which supported bilayers are formed. At low salt concentrations or in water, supported bilayer formation is assumed to proceed via an isolated liposome rupture process that displays little cooperativity (24–26). The presence of salt improves adsorption of liposomes, leading first to their accumulation on the surface to reach a critical density, and then to fusion leading to the formation of supported bilayers through a highly cooperative process (24–26). Alternate models for supported bilayer formation suggest an early rupture process to form a bilayer patch, and subsequent filling up of the interstices by vesicle fusion catalyzed by the bilayer edges around the patch (26–28). Our data support the latter model, as we directly observe membrane patches as a kinetic intermediate during formation of supported bilayers. Of importance, our results indicate that supported bilayers can form with widely different surface densities of liposomes, suggesting that it may not be necessary to reach a critical liposome density for supported bilayer formation.

Our analyses indicate that for supported bilayers formed with negatively charged liposomes, an increase in salt concentration leads to an increase in the membrane reservoir. When formation of supported bilayers is monitored on a glass surface, it can be seen that an increase in salt concentration leads to an increase in both the rate of liposome adsorption and supported bilayer formation. We note, however, that an increase in salt concentration does not cause a proportional increase in the rates of these two processes. Although an increase in salt concentration from 100 mM to 1 M results in a ~6-fold increase in the rate of liposome adsorption, the rate of supported bilayer formation increases by only ~3-fold. The degree of membrane reservoir deposition in supported bilayers is directly related to the product of the rate of liposome adsorption and the characteristic time ($t_{1/2}$) required for supported bilayer formation. The product of these rates for supported bilayers formed at 100 mM NaCl and 1 M NaCl is 37.9 (i.e., 0.5 s^{-1} × 75.8 s; Fig. 3, *C* and *F*) and 65.8 (i.e., 2.8 s^{-1} × 23.5 s; Fig. 3, *C* and *F*), respectively. Thus, an increase in salt concentration from 100 mM to 1 M NaCl results in a 1.7-fold increase in the membrane reservoir in supported bilayers, which matches exactly with our measured value of a 1.7-fold increase in supported bilayers on silica beads formed under these salt concentrations (Fig. 1 *A*). These results indicate that the membrane reservoir in supported bilayers can be predicted by a simple causal relationship between the rate of liposome adsorption and the rate of formation of supported bilayers. Thus, an increase in salt concentration causes a disproportional increase in the rates of these processes, leading to accumulation of excess reservoir with an increase in ionic strength.

We speculate that the cause of the disproportionate increase in rates of adsorption and supported bilayer formation with an increase in salt relates to the manner by which salt influences the balance between liposome adsorption and fusion-induced spreading on the surface. Fusion-induced spreading of liposomes can be considered to be inhibitory to liposome adsorption, since spreading would reduce the area available for liposome binding. Thus, if the kinetics of liposome binding were faster than the kinetics of fusion-induced spreading of liposomes, an initial increase in the liposome density (over that necessary for fusion-induced spreading) would lead to an increase in membrane reservoir because

the finite surface on the silica beads would be covered by more liposomes. Thus, templates with a low reservoir could arise from fewer liposomes thinly spread over the bead surface, and an increase in the capacity for liposome adsorption under such conditions could cause the accumulation of reservoir.

It must be noted that the amount of reservoir in supported bilayers formed with negatively charged lipids at high ionic strength is similar to that seen with zwitterionic lipids formed under conditions of low ionic strength. However, based on its tendency to spontaneously spread out on a glass surface, the reservoir formed with negatively charged supported bilayers appears to be physically less coupled to the underlying silica surface than a zwitterionic supported bilayer. A possible reason for this may be the repulsion experienced by the anionic supported bilayer from the negatively charged silica surface after the charge-screening effect of salt is reduced during washing steps in the course of template preparation. Indeed, the presence of submicroscopic defects in supported bilayers leads to the rapid equilibration of ions across the supported bilayers, which makes them insensitive to osmotic imbalances (18–20).

In summary, we have characterized a template of supported bilayers formed on silica beads in terms of factors that contribute to an increase in the membrane reservoir, an essential criterion for their use in vesicular transport assays. Negatively charged lipids and a high-ionic-strength medium appear to be necessary for this purpose. The templates are a versatile model membrane system because they allow the simultaneous application of biochemical and light-microscopic approaches to analyze membrane-related processes. Because of the relatively simple procedures involved in their preparation, and the fact that they can be formed with a diverse lipid composition, these templates are broadly applicable for reconstituting membrane budding and fission reactions involved in several forms of vesicular transport.

SUPPORTING MATERIAL

One movie is available at http://www.biophysj.org/biophysj/supplemental/S0006-3495(10)00534-5.

We thank Shanti Kalipatnapu, Allen Liu, and Sylvia Neumann for comments on the manuscript.

This work was supported by grants from the National Institutes of Health (R01.GM42455 and R37.MH61345 to S.L.S.) and the Leukemia and Lymphoma Society (5117-08 to T.J.P.). T.J.P. is a fellow of the Leukemia and Lymphoma Society. This is The Scripps Research Institute manuscript No. 20602.

REFERENCES

1. Kirchhausen, T. 2000. Three ways to make a vesicle. *Nat. Rev. Mol. Cell Biol.* 1:187–198.
2. Spang, A. 2008. The life cycle of a transport vesicle. *Cell. Mol. Life Sci.* 65:2781–2789.
3. Pucadyil, T. J., and S. L. Schmid. 2009. Conserved functions of membrane active GTPases in coated vesicle formation. *Science.* 325:1217–1220.
4. Mayor, S., and R. E. Pagano. 2007. Pathways of clathrin-independent endocytosis. *Nat. Rev. Mol. Cell Biol.* 8:603–612.
5. Matsuoka, K., and R. Schekman. 2000. The use of liposomes to study COPII- and COPI-coated vesicle formation and membrane protein sorting. *Methods.* 20:417–428.
6. Takei, K., V. Haucke, …, P. De Camilli. 1998. Generation of coated intermediates of clathrin-mediated endocytosis on protein-free liposomes. *Cell.* 94:131–141.
7. Bashkirov, P. V., S. A. Akimov, …, V. A. Frolov. 2008. GTPase cycle of dynamin is coupled to membrane squeeze and release, leading to spontaneous fission. *Cell.* 135:1276–1286.
8. Ambroggio, E., B. Sorre, …, B. Antonny. 2010. ArfGAP1 generates an Arf1 gradient on continuous lipid membranes displaying flat and curved regions. *EMBO J.* 29:292–303.
9. Groves, J. T., and M. L. Dustin. 2003. Supported planar bilayers in studies on immune cell adhesion and communication. *J. Immunol. Methods.* 278:19–32.
10. Tanaka, M., and E. Sackmann. 2005. Polymer-supported membranes as models of the cell surface. *Nature.* 437:656–663.
11. Kalb, E., S. Frey, and L. K. Tamm. 1992. Formation of supported planar bilayers by fusion of vesicles to supported phospholipid monolayers. *Biochim. Biophys. Acta.* 1103:307–316.
12. Boxer, S. G. 2000. Molecular transport and organization in supported lipid membranes. *Curr. Opin. Chem. Biol.* 4:704–709.
13. Tamm, L. K., and H. M. McConnell. 1985. Supported phospholipid bilayers. *Biophys. J.* 47:105–113.
14. Kiessling, V., and L. K. Tamm. 2003. Measuring distances in supported bilayers by fluorescence interference-contrast microscopy: polymer supports and SNARE proteins. *Biophys. J.* 84:408–418.
15. Pucadyil, T. J., and S. L. Schmid. 2008. Real-time visualization of dynamin-catalyzed membrane fission and vesicle release. *Cell.* 135:1263–1275.
16. McClare, C. W. F. 1971. An accurate and convenient organic phosphorus assay. *Anal. Biochem.* 39:527–530.
17. Ramachandran, R., T. J. Pucadyil, …, S. L. Schmid. 2009. Membrane insertion of the pleckstrin homology domain variable loop 1 is critical for dynamin-catalyzed vesicle scission. *Mol. Biol. Cell.* 20:4630–4639.
18. Giger, K., E. R. Lamberson, and J. S. Hovis. 2009. Formation of complex three-dimensional structures in supported lipid bilayers. *Langmuir.* 25:71–74.
19. Cambrea, L. R., F. Haque, …, J. S. Hovis. 2007. Effect of ions on the organization of phosphatidylcholine/phosphatidic acid bilayers. *Biophys. J.* 93:1630–1638.
20. Cambrea, L. R., and J. S. Hovis. 2007. Formation of three-dimensional structures in supported lipid bilayers. *Biophys. J.* 92:3587–3594.
21. Praefcke, G. J., and H. T. McMahon. 2004. The dynamin superfamily: universal membrane tubulation and fission molecules? *Nat. Rev. Mol. Cell Biol.* 5:133–147.
22. Chappie, J. S., S. Acharya, …, S. L. Schmid. 2009. An intramolecular signaling element that modulates dynamin function in vitro and in vivo. *Mol. Biol. Cell.* 20:3561–3571.
23. Chattopadhyay, A., and E. London. 1984. Fluorimetric determination of critical micelle concentration avoiding interference from detergent charge. *Anal. Biochem.* 139:408–412.
24. Seantier, B., and B. Kasemo. 2009. Influence of mono- and divalent ions on the formation of supported phospholipid bilayers via vesicle adsorption. *Langmuir.* 25:5767–5772.
25. Anderson, T. H., Y. Min, …, J. N. Israelachvili. 2009. Formation of supported bilayers on silica substrates. *Langmuir.* 25:6997–7005.
26. Richter, R. P., R. Bérat, and A. R. Brisson. 2006. Formation of solid-supported lipid bilayers: an integrated view. *Langmuir.* 22:3497–3505.
27. Johnson, J. M., T. Ha, …, S. G. Boxer. 2002. Early steps of supported bilayer formation probed by single vesicle fluorescence assays. *Biophys. J.* 83:3371–3379.
28. Weirich, K. L., J. N. Israelachvili, and D. K. Fygenson. 2010. Bilayer edges catalyze supported lipid bilayer formation. *Biophys. J.* 98:85–92.